Biosensors and Bioelectronics 142 (2019) 111513

Contents lists available at ScienceDirect

Biosensors and Bioelectronics

journal homepage: www.elsevier.com/locate/bios

A signal-off type photoelectrochemical immunosensor for the ultrasensitive detection of procalcitonin: $Ru(bpy)_3^{2+}$ and Bi_2S_3 co-sensitized $ZnTiO_3/TiO_2$ polyhedra as matrix and dual inhibition by SiO_2/PDA-Au

Chunzhu Bao, Dawei Fan*, Xin Liu, Xueying Wang, Dan Wu, Hongmin Ma, Lihua Hu, Huan Wang, Xu Sun, Qin Wei**

Key Laboratory of Interfacial Reaction & Sensing Analysis in Universities of Shandong, School of Chemistry and Chemical Engineering, University of Jinan, Jinan, 250022, PR China

ARTICLE INFO

Keywords:
Signal-off type photoelectrochemical immunosensor
$ZnTiO_3/TiO_2$ polyhedra
$Ru(bpy)_3^{2+}$
Bi_2S_3
SiO_2/PDA-Au
Procalcitonin

ABSTRACT

A signal-off type photoelectrochemical (PEC) immunosensor based on $Ru(bpy)_3^{2+}$ and Bi_2S_3 co-sensitized $ZnTiO_3/TiO_2$ polyhedra as matrix and SiO_2/PDA-Au as the label of second antibody was proposed for the ultrasensitive detection of procalcitonin (PCT). The hollow $ZnTiO_3/TiO_2$ polyhedra called zinc titanium composite hollow structures (ZTCHS) was prepared by hydrothermal method to enhance the utilization of visible light comparing with pure $ZnTiO_3$ or TiO_2. The unique structure endowed large specific surface areas and satisfying load capacity to ZTCHS. $Ru(bpy)_3^{2+}$ and Bi_2S_3 were utilized to co-sensitize ZTCHS to further strengthen the PEC performance of ZTCHS. It was interesting that the dual-inhibition effects of SiO_2/PDA-Au further enhanced the sensitivity of proposed PEC immunosensor. On the one hand, the steric hindrance of SiO_2/PDA effectively restricted electron transfer. On the other hand, Au nanoparticles could absorb visible light to compete with the matrix material. Based on the above aspects, the proposed signal-off type PEC immunosensor possessed a wide linear range from 0.0001 ng mL^{-1} to 100 ng mL^{-1} and low detection limit (about 0.03 pg mL^{-1}, S/N = 3), demonstrating the promising application of PEC immunosensor in analysis fields.

1. Instruction

Photoelectrochemical (PEC) immunosensor has been became a high-profile analysis method in the diagnosis of disease, the detection of food safety, environmental protection and other fields (Li et al., 2018a; Mao et al., 2019; Yan et al., 2018a; Zhou et al., 2018). By immobilizing sensitive biomaterials such as enzymes, antigens, antibodies, DNA and other active substances to as the recognition element, PEC immunosensor outputs the signal expressed by sensitive biomaterials to as electrical signals. The specific recognition of biomaterials endows PEC immunosensor excellent specificity and sensitivity for the diagnosis of cancer. However, how to construct a stabilized photoelectric sensing material interface and design the outstanding construction strategy is still an important challenge and one of the scientific problems to be solved.

As the promising metallic oxide materials, $ZnTiO_3$ and TiO_2 have attracted interest of numerous researchers due to the unique property such as the satisfying chemical stability, non-toxicity, excellent photoelectric activity, high quantum efficiency and redox ability (Giampiccolo et al., 2019; Sun et al., 2018; Tian et al., 2017; Yan et al., 2018b). However, the wide band-gap of $ZnTiO_3$ and TiO_2 hinders the separation of photo-generated electrons and holes, reducing the conversion efficiency of photocurrent. Nowadays, some reports have coupled the $ZnTiO_3$ and TiO_2 with other semiconductors or doped elements to solve the above limitation. For example, researchers have constructed ZnO/$ZnTiO_3$ nanoheterostructures, ZnO nanorods/TiO_2 hierarchical heterostructure films and La–TiO_2 heterostructure to enhance the PEC performance of $ZnTiO_3$ or TiO_2 (Ali et al., 2017; Fan et al., 2017; Ranjith and Uyar, 2018; Zhao et al., 2019). In our work, the novel hollow $ZnTiO_3/TiO_2$ polyhedra called zinc titanium composite hollow structures (ZTCHS) is employed by hydrothermal method to enhance the utilization of visible light (Tian et al., 2017). Comparing with the pure $ZnTiO_3$ or TiO_2, the ZTCHS possesses excellent stability, large specific surface areas and capacity, satisfying load capacity and so on, which is benefit to the loading of nanoparticles.

As a kind of luminous reagent, $Ru(bpy)_3^{2+}$ with satisfying physical

* Corresponding author.
** Corresponding author.
E-mail addresses: jndxfandawei@126.com (D. Fan), sdjndxwq@163.com (Q. Wei).

https://doi.org/10.1016/j.bios.2019.111513
Received 8 May 2019; Received in revised form 25 June 2019; Accepted 12 July 2019
Available online 13 July 2019
0956-5663/

and chemical properties has attracted the interest of many scholars. For example, Liao et al. have constructed linear $Ru(bpy)_3^{2+}$-Polymer to as the probe for the detection of biomarkers (Liao et al., 2017). Li et al. have combined hyaluronic acid with $Ru(bpy)_3^{2+}$ to detect hyaluronidas (Li et al., 2018b). Wu et al. have prepared phosphonate-substituted ruthenium (II) bipyridyl derivative to as the PEC probe (Wu et al., 2018). In our work, $Ru(bpy)_3^{2+}$ is modified on the surface of ZTCHS polyhedra by the electrostatic interaction to sensitize the materials due to excellent conductivity and satisfying PEC properties. Under the irradiation of visible light, $Ru(bpy)_3^{2+}$ is oxidized to Ru(III) complex and then become to the excited state Ru(II)*. Subsequently, Ru(II)* returns to the ground state and produces a strong electrochemiluminescence (ECL) emission with electron transfer and energy transfer, improving the PEC performance of materials.

Moreover, bismuth sulfide (Bi_2S_3) with outstanding PEC activity is used to further sensitize ZTCHS. On the one hand, the band-gap of Bi_2S_3 is about 1.30–1.70 eV, which is benefit to the separation of photogenerated electrons and holes, enhancing the intensity of photocurrent signal (Paul et al., 2017; Shi et al., 2018; Wang et al., 2018). On the other hand, the perfect match of band-gap between Bi_2S_3 and ZTCHS accelerates efficiently the electron transfer, improving the utilization of visible light. Based on the above discussions, $Ru(bpy)_3^{2+}$ and Bi_2S_3 are used to co-sensitize ZTCHS to form the ZTCHS/$Ru(bpy)_3^{2+}$/Bi_2S_3 material which is proposed as matrix material of PEC immunosensor due to the excellent PEC performance.

After solving the problem of stabilized photoelectric sensing material interface, it is the most important to design the outstanding construction strategy. In order to achieve the ultrasensitive detection, the signal-off type PEC immunosensor is proposed based on an outstanding quenching agent. At first, as a stable semiconductor material, SiO_2 plays a significant role in catalytic degradation, lithium batteries and other fields (Deveci and Mercimek, 2019; Liu et al., 2017; Tang et al., 2018). Meanwhile, the large steric hindrance and poor conductivity of SiO_2 hinder the electron transfer and reduce the PEC activity of immunosensor, which proves the status of SiO_2 as a quenching agent (Xu et al., 2018; Zhang et al., 2018). Secondly, as a kind of highly regarded metal nanoparticle, Au nanoparticles absorb the visible light resulting in the energy transfer (Dou et al., 2017; Lu et al., 2019; Sun et al., 2017). And Au nanoparticles facilitate the close combination of the materials and secondary antibody (Ab_2) because of the firm Au–NH_2 bond. Finally, dopamine hydrochloride is grown on the surface of SiO_2 to form a polydopamine (PDA) coating layer, which is beneficial to the connection between SiO_2 and Au nanoparticles, and achieves higher quenching efficiency. Thus, SiO_2/PDA-Au is proposed as the label of Ab_2 to construct the signal-off type PEC immunosensor, realizing the ultrasensitive of procalcitonin (PCT).

According to the analysis, septicemia is one of the major causes result in the high mortality all over the world. PCT is widely believed to be an effective biomarker for early septicemia diagnosis (Fang et al., 2018; Seshadri et al., 2018; Shen et al., 2015). The concentration of PCT is less than 0.1 ng mL^{-1} in the healthy human serum, and increase to 1.00 ng mL^{-1} or more than 10.0 ng mL^{-1} in the serum of patients with septicemia, which indicates that it is vital to detect PCT sensitively (Ghrera, 2019; Liu et al., 2014; Sui et al., 2018). Therefore, in our work, a signal-off type PEC immunosensor based on $Ru(bpy)_3^{2+}$ and Bi_2S_3 co-sensitized $ZnTiO_3/TiO_2$ polyhedra as matrix and dual inhibition by SiO_2/PDA-Au is proposed to achieve the ultrasensitive detection of PCT.

2. Experimental

2.1. Materials and reagents

PCT, primary antibody (Ab_1) and Ab_2 were obtained from Shanghai Linc-Bio Science Co., Ltd, China. Other details were indicated in Supporting Information.

2.2. Apparatus

A LED lamp (100 W, white light) was utilized as an irradiation source in the PEC tests, and the wavelength range of that was shown in Fig. S1. Other details were shown in Supporting Information.

2.3. Synthesis of ZTCHS

According to the previous reported literature (Tian et al., 2017), ZTCHS was synthesis by hydrothermal method. And the details were shown in Supporting Information.

2.4. Preparation of SiO_2/PDA-Au nanoparticles

The SiO_2/PDA-Au nanoparticles were synthesized as follows. Sodium citrate (0.0244 g) was dissolved in 40 mL ultrapure water. After adding 2% $HAuCl_4$ (40 μL) and 5 mg PDA@SiO_2 (the synthesis process of PDA@SiO_2 was showed in Supporting Information), the obtained solution was stirred for 5 min. And then, the solution was heated and boiled for 15 min. After cooling to room temperature, the solution was centrifuged and washed with ultrapure water for several times to obtain SiO_2/PDA-Au nanoparticles.

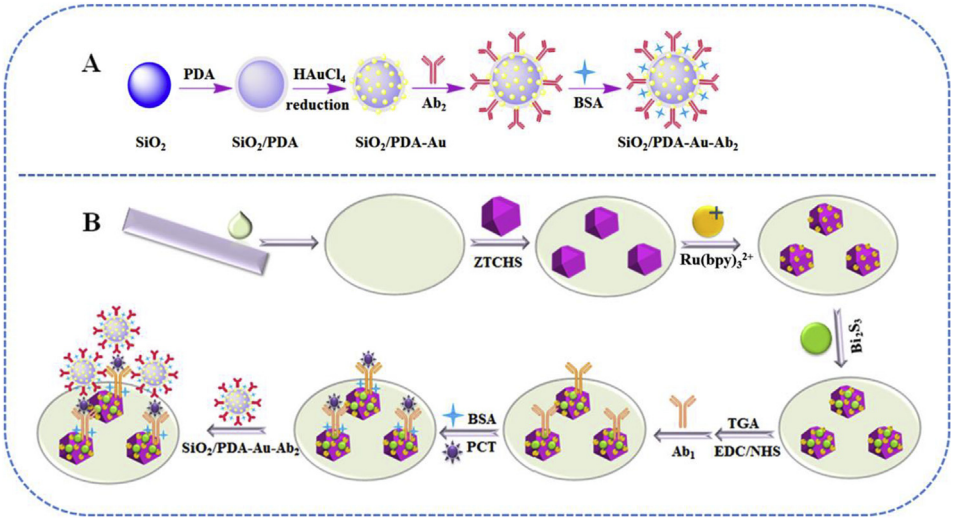

Scheme 1. Preparation process of the SiO_2/PDA-Au-Ab_2 conjugate and construction process of the proposed PEC immunosensor.

2.5. Synthesis of SiO_2/PDA-Au-Ab_2

As shown in Scheme 1A, the SiO_2/PDA-Au-Ab_2 conjugate was prepared as follows: 5 mg of SiO_2/PDA-Au was added to PBS solution (1 mL, pH = 7.4). Subsequently, the Ab_2 solution (10 μg mL^{-1}, 200 μL) was added to the above solution and then incubated for 2 h at 30 °C. Washing with PBS (pH = 7.4), the obtained product was dissolved into 1 mL PBS (pH = 7.4, containing 0.1% BSA) and then stored at 4 °C for the further use.

2.6. Construction of signal-off type PEC immunosensor

Scheme 1B explicitly showed the construction process of the proposed PEC immunosensor. At first, under the ultrasound condition, the indium tin oxide (ITO) electrode was cleared using acetone, ethanol and ultrapure water, respectively. The ITO electrode was dried for 2 h at 70 °C. Then, the ZTCHS (10 μL, 4 mg mL^{-1}) was dropped on the prepared ITO electrode to form ITO/ZTCHS electrode. In order to stabilize the photocurrent signal of ITO/ZTCHS electrode, the electrode was calcined for 30 min at 450 °C. After the preparation step of ITO/ZTCHS electrode, it was noteworthy that each modified layer of the electrodes needs to be washed with ultrapure water and dried at room temperature. The 0.03 mol L^{-1} of $Ru(bpy)_3^{2+}$ solution (4 μL) was modified on the surface of ZTCHS to enhance the PEC activity of material. It was important to note that the process required doing in the dark. Using the simple in-situ growth method, the dilute nitric acid solution of $Bi(NO_3)_3$ (4 μL, 0.03 mol L^{-1}) was modified on the above electrode. After dropping the excessive Na_2S on the above electrode, the Bi^{3+} immediately reacted with S^{2+} to generate Bi_2S_3 nanoparticles forming ITO/ZTCHS/$Ru(bpy)_3^{2+}$/Bi_2S_3 electrode. As the ideal coupling agent, the 0.1 mol L^{-1} of TGA (4 μL) was fixed to the electrode using the combine between sulfydryl and Bi^{3+}. The 4 μL of EDC/NHS (10 mmol L^{-1}/ 2 mmol L^{-1}) was added to the electrode to activate the –COOH of TGA. Through the combination between –COOH of TGA and –NH_2 of Ab_1, 4 μL of Ab_1 (1 μg mL^{-1}) was immobilized on the above electrode. And then, 0.1% BSA (5 μL) solution was used to block the nonspecific sites. Subsequently, the different concentrations of PCT (4 μL) were added to the above electrode, which generated various photocurrent signals. Finally, 4 μL of SiO_2/PDA-Au-Ab_2 solution was modified on the above electrode to construct the signal-off type ITO/ZTCHS/$Ru(bpy)_3^{2+}$/Bi_2S_3/TGA/(EDC/NHS)/Ab_1/BSA/PCT/(SiO_2/PDA-Au-Ab_2) PEC immunosensor.

3. Results and discussion

3.1. Characterization of synthetic materials

Firstly, the SEM, TEM and EDS images of synthetic materials were measured to explore the morphology and elementary composition. As the template, ZIF-8 was solid polyhedral indicated by the SEM (Fig. 1A) and TEM (Fig. 1B) images. After disposing ZIF-8 through the hydrothermal method, the unique ZTCHS polyhedral was prepared, which was proved by the SEM (Fig. 1C) and TEM (Fig. 1D) images of ZTCHS. And the size of ZTCHS was about 200 nm contributing to the loading of nanoparticles. After $Ru(bpy)_3^{2+}$ and Bi_2S_3 co-sensitized the ZTCHS, the surface of ZTCHS loaded many small nanoparticles (Fig. 1E), which indicated the ZTCHS/$Ru(bpy)_3^{2+}$/Bi_2S_3 was prepared successfully. Comparing with the EDS data of ZTCHS (Fig. S2A and Table S1), the EDS data of ZTCHS/$Ru(bpy)_3^{2+}$/Bi_2S_3 had Ru, Bi and S elements (Fig. S2B and Table S2), which further improved the successful preparation of ZTCHS/$Ru(bpy)_3^{2+}$/Bi_2S_3 materials. Fig. 1F and G were the SEM images of SiO_2 and SiO_2/PDA. It was obvious that after modifying with PDA, the surface of uniform SiO_2 was covered with thin film. And there are many Au nanoparticles in the SEM image of SiO_2/PDA-Au (Fig. 1H). Combining with the EDS data of SiO_2/PDA-Au (Fig. S2C and Table S3), it was further illustrated the successful preparation of SiO_2/PDA-Au.

In Fig. S3, the XRD pattern of ZIF-8 was consistent with the literature (Tian et al., 2017), which further improved the successful preparation of ZIF-8. The XRD patterns of uncalcinated (a) and calcined (b) ZTCHS materials were compared in Fig. 2A, which indicated both of the diffraction peaks could match well with the standard spectrum (PDF#39–0190). And the diffraction peaks of ZTCHS/$Ru(bpy)_3^{2+}$/Bi_2S_3 (c) could be consistent with the standard spectrum of Bi_2S_3 (PDF#17–0320). It could be seen that the diffraction peaks of Bi_2S_3 were so strong that they hided the diffraction peaks of ZTCHS. Moreover, in the XRD patterns of SiO_2, SiO_2/PDA and SiO_2/PDA-Au (Fig. 2B), the diffraction peaks could match well with the standard spectrums of SiO_2 (PDF#39–1425) and Au (PDF#04–0784). In a word, the above data indicated that ZTCHS/$Ru(bpy)_3^{2+}$/Bi_2S_3 and SiO_2/PDA-Au were prepared successfully.

Observing the UV–vis diffuse reflectance spectra of ZTCHS (Fig. 2C and D), the data indicated that ZTCHS had certain absorbance range and intensity to visible light, and the band-gap energy of ZTCHS was calculated to 3.60 eV. The result manifested that the absorbance capacity of ZTCHS to visible light was limited, and the wide band-gap impeded the separation efficiency of photo-generated electron-hole. Moreover, the PL emission spectra of ZTCHS (curve a), ZTCHS/$Ru(bpy)_3^{2+}$ (curve b) and ZTCHS/$Ru(bpy)_3^{2+}$/Bi_2S_3 (curve c) were studied under the excitation wavelength of 315 nm. The weak intensity of PL emission means the strong photocurrent signal. As shown in Fig. 2E, the PL emission intensity of ZTCHS/$Ru(bpy)_3^{2+}$/Bi_2S_3 was obviously weaker than that of ZTCHS and ZTCHS/$Ru(bpy)_3^{2+}$ on the whole, which manifested the ZTCHS/$Ru(bpy)_3^{2+}$/Bi_2S_3 possessed the excellent PEC activity. And it is obvious that the SiO_2/PDA-Au has certain absorption to the visible light in the range from 300 nm to 800 nm (curve f), which distinctly stronger than that of SiO_2/PDA (curve e) and Au nanoparticles (curve d).

3.2. Characterization of signal-off type PEC immunosensor

As shown in Fig. 3, the Time-Photocurrent curves (A and B) and EIS Nyquist plots (C) of the each layer of PEC immunosensor were researched to detect the construction of PEC immunosensor. In Fig. 3A, after ZTCHS was coated on the ITO electrode (curve b) and $Ru(bpy)_3^{2+}$ (curve c) sensitized ZTCHS materials, the photocurrent signals gradually increased comparing with pure ITO electrode (curve a). Using the in-situ growth method, the photocurrent signal of ITO/ZTCHS/Ru$(bpy)_3^{2+}$/Bi_2S_3 electrode increased to about 85 μA (curve d) that was almost eighty five times that of pure ZTCHS. In order to combine Ab_1, TGA and EDC/NHS were modified on the ITO/ZTCHS/$Ru(bpy)_3^{2+}$/Bi_2S_3 electrode, and then the photocurrent signal of above electrode decreased because of the inhibition effect of organic molecular (curve e). Subsequently, with the modification of Ab_1 (curve f), BSA (curve g) and PCT (curve h), the photocurrent signals gradually diminished due to the outstanding insulation of protein molecules. After modifying SiO_2/PDA-Au-Ab_2 on the above electrode, the steric hindrance effect of SiO_2/PDA and absorption ability to visible light of Au distinctly decreased the photocurrent signal (curve i).

In Fig. 3C, EIS Nyquist plots was researched in 5.0 mmol L^{-1} of $[Fe(CN)_6]^{3-/4-}$ solution (containing 0.1 mol L^{-1} of KCl) to deeply analyze the construction processes of each layer PEC immunosensor. The diameter of the semicircle part in EIS Nyquist plots usually reports the electron transfer resistance (R_{et}) value (Fan et al., 2016). After modifying the ZTCHS (curve b), $Ru(bpy)_3^{2+}$ (curve c) and Bi_2S_3 (curve d), the R_{et} values gradually increased comparing with pure ITO electrode (curve a) due to the obstacle effect of materials. And the data were consistent with the Time-Photocurrent curves, which convincingly certified that the ITO/ZTCHS/$Ru(bpy)_3^{2+}$/Bi_2S_3 electrode was constructed successfully. Afterwards, TGA and EDC/NHS were dropped on the above electrode, which impeded electron transfer and increased the R_{et} values of electrode (curve e). And the modification of Ab_1 (curve f), BSA (curve g) and PCT (curve h) also magnified the R_{et} values of

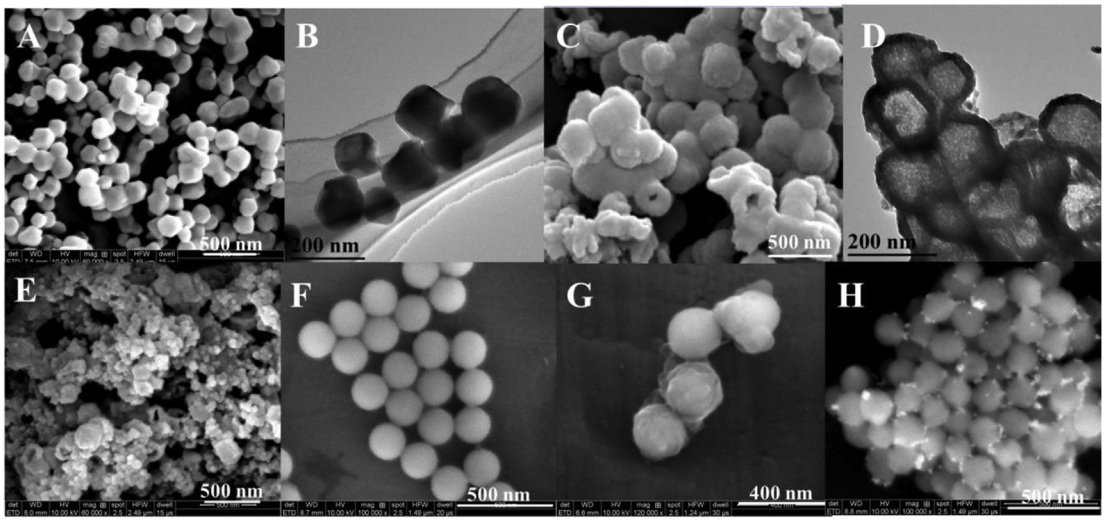

Fig. 1. SEM (A) and TEM (B) images of ZIF-8. SEM (C) and TEM (D) images of ZTCHS. SEM images of ZTCHS/Ru(bpy)$_3^{2+}$/Bi_2S_3 (E), SiO_2 (F), SiO_2/PDA (G), SiO_2/PDA-Au (H).

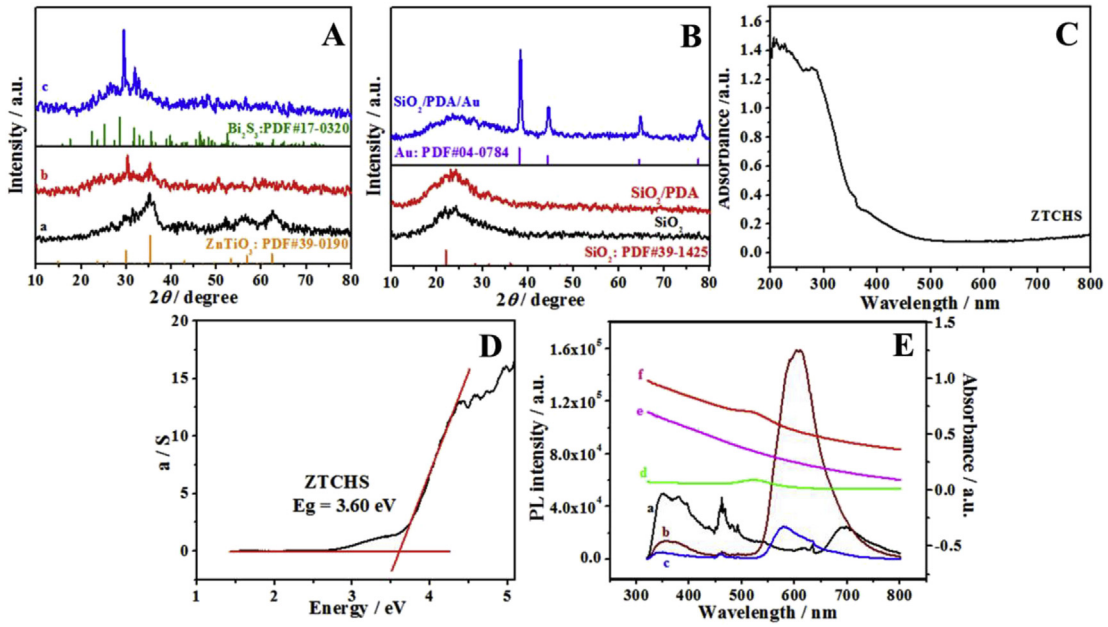

Fig. 2. (A) XRD patterns of uncalcinated ZTCHS (a), calcined ZTCHS (b) and ZTCHS/Ru(bpy)$_3^{2+}$/Bi_2S_3 (c). (B) XRD patterns of SiO_2, SiO_2/PDA and SiO_2/PDA-Au. (C) and (D) UV–vis diffuse reflectance spectra of ZTCHS. (E) PL emission spectra of ZTCHS (a), ZTCHS/Ru(bpy)$_3^{2+}$ (b) and ZTCHS/Ru(bpy)$_3^{2+}$/Bi_2S_3 (c) and UV–Vis spectrum of Au nanoparticles (d), SiO_2/PDA (e) and SiO_2/PDA-Au (f).

electrode because of the hindrance and insulation property of protein. Finally, SiO_2/PDA-Au-Ab_2 was modified on the electrode resulting in the significant enlargement of R_{et} values (curve i), which effectively indicated the successful construction of signal-off type PEC immunosensor.

The electron transfer mechanism of fabricated PEC immunosensor was showed in Fig. 3D. According to the UV–vis diffuse reflectance spectra (Fig. 2D), ZTCHS possessed wide band-gap (3.60 eV), which hindered the separation of photo-generated electron-hole. Previous literature reported that Bi_2S_3 generated by the in-situ grown method had the narrow band-gap (about 1.64 eV) (Fan et al., 2018). Thus, Bi_2S_3 was generated on the surface of ZTCHS to adjust the band-gap of materials and enhance the efficiency of electron transfer. Moreover, the conduction band (CB) of ZTCHS and Bi_2S_3 were calculated to 0.76 V and 0.12 V, the valence band (VB) of that were 4.36 V and 1.76 V according to the Mott-Schottky curves of ZTCHS and Bi_2S_3 (Figs. S4A and B). The well match of band-gap between ZTCHS and Bi_2S_3 was benefiting for the absorbance to visible light, accelerating the electron transfer. Under irradiation of visible light, the photo-generated electrodes transferred from VB of Bi_2S_3 to CB, and then transferred to the CB of ZTCHS because of the interfacial adhesion. Meanwhile, Ru(bpy)$_3^{2+}$ was oxidized to Ru(III) complex. Ru(III) complex reacted with ZTCHS and then became to the excited state Ru(II)*. Along with electron transfer and energy transfer, Ru(II)* returned to the ground state and produced a strong ECL emission, which further improved the PEC performance of materials (Fan et al., 2019; Hong et al., 2017). Thus, Ru(bpy)$_3^{2+}$ and Bi_2S_3 co-sensitized ZTCHS adequately absorbed visible light and expressed the outstanding photocurrent signal. In addition, SiO_2/PDA-Au was designed as the label of Ab_2 to achieve the ultrasensitive detection of PCT. On the one hand, the steric hindrance of SiO_2/PDA effectively restricted electron transfer. On the other hand, Au nanoparticles, as a competitor, could absorb visible light due to the

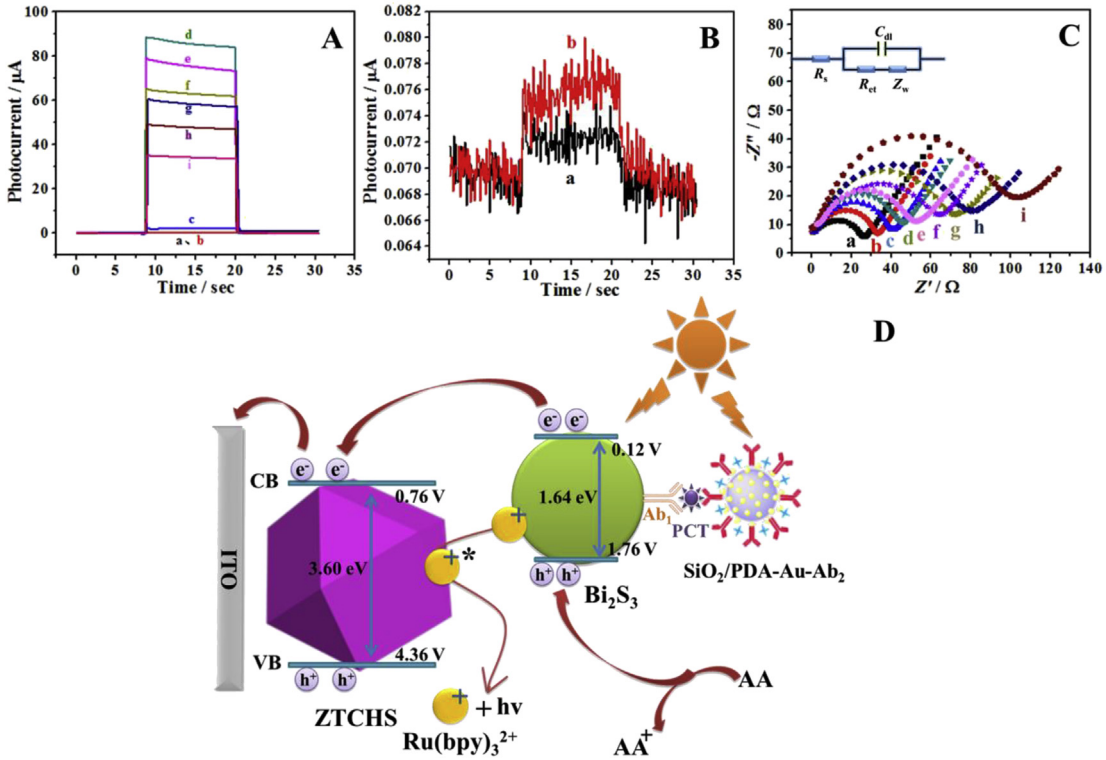

Fig. 3. (A and B) Time-Photocurrent curves and (C) EIS Nyquist plots of each layer of PEC immunosensor, (a) ITO, (b) ITO/ZTCHS, (c) ITO/ZTCHS/$Ru(bpy)_3^{2+}$, (d) ITO/ZTCHS/$Ru(bpy)_3^{2+}$/Bi_2S_3, (e) ITO/ZTCHS/$Ru(bpy)_3^{2+}$/Bi_2S_3/TGA/(EDC/NHS), (f) ITO/ZTCHS/$Ru(bpy)_3^{2+}$/Bi_2S_3/TGA/(EDC/NHS)/Ab_1, (g) ITO/ZTCHS/$Ru(bpy)_3^{2+}$/Bi_2S_3/TGA/(EDC/NHS)/Ab_1/BSA, (h) ITO/ZTCHS/$Ru(bpy)_3^{2+}$/Bi_2S_3/TGA/(EDC/NHS)/Ab_1/BSA/PCT, (i) ITO/ZTCHS/$Ru(bpy)_3^{2+}$/Bi_2S_3/TGA/(EDC/NHS)/Ab_1/BSA/PCT/(SiO_2/PDA-Au-Ab_2). The inset in C was Randles equivalent circuit for EIS. The applied potential is 0 V. (D) Electron transfer mechanism of fabricated signal-off type PEC immunosensor.

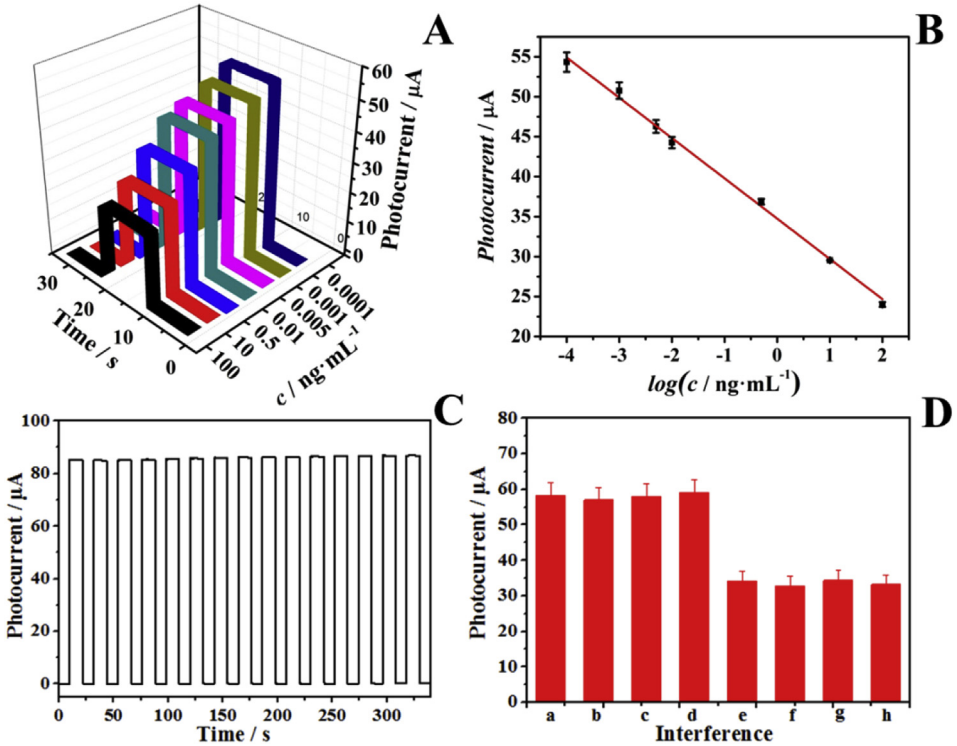

Fig. 4. (A) Photocurrent responses of proposed PEC immunosensor with different concentrations of PCT. (B) The logarithmic calibration curve of proposed PEC immunosensor to detect different concentrations of PCT. (C) Under several on/off irradiation cycles for 350 s, Time-based photocurrent responses of proposed PEC immunosensor (c_{PCT} = 1 ng mL^{-1}) (D) The specificity of the proposed PEC immunosensor to detect PCT. (a) Blank, (b) blank + 100 ng mL^{-1} SCCA, (c) blank + 100 ng mL^{-1} cTnI, (d) blank + 100 ng mL^{-1} NT-proBNP, (e) 1 ng mL^{-1} PCT, (f) 1 ng mL^{-1} PCT +100 ng mL^{-1} SCCA, (g) 1 ng mL^{-1} PCT +100 ng mL^{-1} cTnI, (h) 1 ng mL^{-1} PCT +100 ng mL^{-1} NT-proBNP.

Table 1
The results of the PCT determination in human serum sample.

Serum sample	Addition PCT concentration ($ng{\cdot}mL^{-1}$)	Detection average value ($ng{\cdot}mL^{-1}$)		RSD (%, n = 5)		Recovery (%, n = 5)		Relative errors (%)
		Our method	ELISA	Our method	ELISA	Our method	ELISA	
0.003	1.00×10^{-2}	1.05×10^{-2}	1.04×10^{-2}	3.70	3.22	105	104	0.962
	1.00×10^{-1}	0.958×10^{-1}	0.943	3.53	3.61	95.8	94.3	1.59
	1.00	0.975	1.01	2.65	2.57	97.5	101	−3.47
	5.00	5.16	4.97	2.71	2.49	103	97.4	3.82
	10.0	10.3	10.1	2.30	1.88	103	101	1.98

overlap between the LED light resource (Fig. S1) and the UV–Vis spectrum of Au (Fig. 2E). And the overlap between the emission wavelength of ZTCHS/Ru(bpy)$_3^{2+}$/Bi_2S_3 and the absorbance range of Au greatly facilitated the exciton recombination reducing the PEC activity of ZTCHS/Ru(bpy)$_3^{2+}$/Bi_2S_3 (Bao et al., 2018). As the excellent electron donor, AA eliminated electrode holes to ensure the stability of photocurrent in the whole process.

3.3. Optimization of experimental conditions

The optimization of experimental conditions was benefit for the PEC immunosensor to perform optimally. Thus, the calcined temperature of ZTCHS, concentration of $Bi(NO_3)_3$ and SiO_2/PDA-Au, concentration of AA and pH in the PBS buffer solution were explored in Fig. S5. It was vital for ZTCHS to choose the suitable calcined temperature. Higher temperature could destroy the morphology of ZTCHS and oxidize ZTCHS to Zn_2TiO_4 or other oxides. Lower temperature could not endow ZTCHS excellent stability. As showed in Fig. S5A, the most appropriate temperature was 450 °C. In addition, the concentration of material was one of the important factors affecting PEC immunosensor performance. Insufficient materials and excessive materials leaded to poor performance of PEC immunosensor. As shown in Fig. S5B, C and D, the optimal concentrations of $Bi(NO_3)_3$, SiO_2/PDA-Au and AA were 0.03 mol L^{-1}, 5 mg mL^{-1} and 0.10 mol L^{-1}. Moreover, the acidity-alkalinity of pH had significant influence on the performance of PEC immunosensor. The data indicated that the PEC immunosensor expressed optimal PEC activity under the condition of pH 7.4. The result could be explained that pH of 7.4 was similar with the physiological environment contributing to the expression of immobilized proteins.

3.4. Photoelectrochemical analysis for proposed PEC immunosensor

Under the optimal condition, the PEC immunosensor was proposed and analyzed the performance. As shown in Fig. 4A, the obtained photocurrent signals were different with various concentrations of PCT. And the logarithmic calibration curve was drawn using the relationship between concentration and signal in Fig. 4B. In the concentration range from 0.0001 ng mL^{-1} to 100 ng mL^{-1}, the regression equation of the calibration curve was $I = 34.75–5.041\ lgc$ ($ng{\cdot}mL^{-1}$) with the linear coefficient of 0.9965. And the detection limit (LOD, S/N = 3) was about 0.03 pg mL^{-1}, which was obviously superior to other reported methods for detection of PCT according to Table S4 (the data and other details were shown in the Supporting Information) achieving the ultrasensitive detection for PCT.

In order to further analyze the performance, the stability of PEC immunosensor was explored under several on/off irradiation cycles for 350 s. As shown in Fig. 4C, there was no obvious change for photocurrent signal. After the proposed PEC immunosensor was stored for 3 weeks in a refrigerator (4 °C), 92.5% of its initial photocurrent signal could be obtained to detect PCT. Based on the above aspects, the proposed PEC immunosensor possessed satisfactory stability. Subsequently, the photocurrent signals of five electrodes (modified under the same conditions) were investigated to research the reproducibility of the prepared PEC immunosensor. The result was 34.13 μA, 33.25 μA, 35.41 μA, 36.23 μA and 34.89 μA. And the relative standard deviation (RSD) was calculated as 3.3%, which proved the prepared PEC immunosensor possessed the excellent reproducibility. Fig. 4D demonstrated the selectivity of the prepared PEC immunosensor. Even if interfering substances of squamous cell carcinoma antigen (SCCA), cardiac troponin I (cTnI) and N-terminal pro-B-type natriuretic peptide (NT-proBNP) were incubated on the blank electrodes (ITO/ZTCHS/Ru(bpy)$_3^{2+}$/Bi_2S_3/TGA/(EDC/NHS)/Ab_1/BSA electrode), the obtained photocurrent signals were no significantly change comparing with the blank electrode without interfering substances. After 1 ng mL^{-1} of PCT mixed with interfering substances (100 ng mL^{-1}) and incubated on the designed PEC immunosensor, the measured signals were similar to that of the designed PEC immunosensor without interfering substances, proving the outstanding selectivity of the prepared PEC immunosensor.

3.5. Real sample analysis

As shown in Table 1, the concentrations of PCT in human blood serum samples were measured by standard addition methods to appraise the practicability of the proposed PEC immunosensor. The result indicated that the RSD and recoveries of the serum samples were in the range of 2.30–3.70% and 95.8–105%, respectively. Subsequently, the classical enzyme-linked immunosorbent assay (ELISA) method was used to detect PCT in serum sample to further improve the accuracy of the signal-off type PEC immunosensor. It was satisfying that the results of the two detection methods were basically consistent, manifesting the promising analytical application of the constructed PEC immunosensor.

4. Conclusion

In conclusion, $ZnTiO_3$/TiO_2 polyhedra (ZTCHS) with unique hollow structure were prepared by hydrothermal method to enhance the utilization of visible light comparing with pure $ZnTiO_3$ or TiO_2. Ru(bpy)$_3^{2+}$ was utilized to sensitize ZTCHS to accelerate the electron transfer. By the in-situ growth method, Bi_2S_3 was further used to sensitize ZTCHS to form ZTCHS/Ru(bpy)$_3^{2+}$/Bi_2S_3 with satisfying PEC activity. In addition, the steric hindrance of SiO_2/PDA and the absorption capacity of Au nanoparticles to visible light effectively restricted the PEC performance of matrix materials. Therefore, using ZTCHS/Ru(bpy)$_3^{2+}$/Bi_2S_3 as matrix and SiO_2/PDA-Au as the label of Ab_2, a signal-off strategy PEC immunosensor was proposed. And the constructed PEC immunosensor expressed a wide linear range (0.0001–100 ng mL^{-1}) and low detection limit (0.03 pg mL^{-1}, S/N = 3), revealing hopeful actual applications in analytical fields.

Declaration of competing interest

☒√The authors declare that they have no known competing financial interests or personal relationships that could have appeared to influence the work reported in this paper.

CRediT authorship contribution statement

Chunzhu Bao: Conceptualization, Data curation, Writing - original

draft. **Dawei Fan:** Methodology, Data curation, Writing - review & editing. **Xin Liu:** Methodology, Writing - review & editing. **Xueying Wang:** Methodology. **Dan Wu:** Formal analysis. **Hongmin Ma:** Formal analysis. **Lihua Hu:** Formal analysis. **Huan Wang:** Funding acquisition, Formal analysis. **Xu Sun:** Formal analysis. **Qin Wei:** Funding acquisition, Formal analysis.

Acknowledgments

This research was financially supported by the National Natural Science Foundation of China (Nos., 21605094, 21607055, 21601064, 21575050), the Natural Science Foundation of Shandong Province (No. ZR2017BB030, ZR2016BQ10), the National Key Scientific Instrument and Equipment Development Project of China (No. 21627809), and QW thanks the Special Foundation for Taishan Scholar Professorship of Shandong Province (No. ts20130937) and UJN.

Appendix A. Supplementary data

Supplementary data to this article can be found online at https://doi.org/10.1016/j.bios.2019.111513.

References

Ali, A., Li, X., Song, J., Yang, S., Zhang, W., Zhang, Z., Xia, R., Zhu, L., Xu, X., 2017. J. Phys. Chem. C 121, 21096–21104.
Bao, C., Wang, C., Fan, D., Ma, H., Hu, L., Fan, Y., Wei, Q., 2018. New J. Chem. 42, 15762–15769.
Deveci, İ., Mercimek, B., 2019. Ultrason. Sonochem. 51, 197–205.
Dou, Y., Zhou, J., Zhou, A., Li, J.-R., Nie, Z., 2017. J. Mater. Chem. 5, 19491–19498.
Fan, D., Bao, C., Liu, X., Wu, D., Zhang, Y., Wang, H., Du, B., Wei, Q., 2018. J. Mater. Chem. B 6, 7634–7642.
Fan, D., Liu, X., Bao, C., Feng, J., Wang, H., Ma, H., Wu, D., Wei, Q., 2019. Biosens. Bioelectron. 129, 124–131.
Fan, D., Ren, X., Wang, H., Wu, D., Zhao, D., Chen, Y., Wei, Q., Du, B., 2017. Biosens. Bioelectron. 87, 593–599.
Fan, G.C., Zhu, H., Du, D., Zhang, J.R., Zhu, J.J., Lin, Y., 2016. Anal. Chem. 88, 3392–3399.
Fang, Y., Hu, Q., Yu, X., Wang, L., 2018. Sens. Actuators, B 258, 238–245.
Ghrera, A.S., 2019. Anal. Chim. Acta 1056, 26–33.
Giampiccolo, A., Tobaldi, D.M., Leonardi, S.G., Murdoch, B.J., Seabra, M.P., Ansell, M.P., Neri, G., Ball, R.J., 2019. Appl. Catal., B 243, 183–194.
Hong, L.-R., Zhao, J., Lei, Y.-M., Yuan, R., Zhuo, Y., 2017. Electrochim. Acta 241, 291–298.
Li, L., Wang, T., Zhang, Y., Xu, C., Zhang, L., Cheng, X., Liu, H., Chen, X., Yu, J., 2018a. ACS Appl. Mater. Interfaces 10, 14594–14601.
Li, Z., Chen, H., Zhuo, Z., Huang, D., Luo, F., Chen, L., Wang, J., Guo, L., Qiu, B., Lin, Z., 2018b. Sens. Actuators, B 275, 409–414.
Liao, Y., Zhou, X., Fu, Y., Xing, D., 2017. Anal. Chem. 89, 13016–13023.
Liu, F., Xiang, G., Yuan, R., Chen, X., Luo, F., Jiang, D., Huang, S., Li, Y., Pu, X., 2014. Biosens. Bioelectron. 60, 210–217.
Liu, Y., Wei, R., Lin, O., Zhang, W., Du, Y., Wang, C., Zhang, C., 2017. ACS Sustain. Chem. Eng. 5, 7812–7823.
Lu, M., Zhu, H., Bazuin, C.G., Peng, W., Masson, J.F., 2019. ACS Sens. 4, 613–622.
Mao, L., Ji, K., Yao, L., Xue, X., Wen, W., Zhang, X., Wang, S., 2019. Biosens. Bioelectron. 127, 57–63.
Paul, S., Ghosh, S., Barman, D., De, S.K., 2017. Appl. Catal., B 219, 287–300.
Ranjith, K.S., Uyar, T., 2018. ACS Sustain. Chem. Eng. 6, 12980–12992.
Seshadri, P., Manoli, K., Schneiderhan-Marra, N., Anthes, U., Wierzchowiec, P., Bonrad, K., Di Franco, C., Torsi, L., 2018. Biosens. Bioelectron. 104, 113–119.
Shen, W.J., Zhuo, Y., Chai, Y.Q., Yang, Z.H., Han, J., Yuan, R., 2015. ACS Appl. Mater. Interfaces 7, 4127–4134.
Shi, Y., Xiong, X., Ding, S., Liu, X., Jiang, Q., Hu, J., 2018. Appl. Catal., B 220, 570–580.
Sui, Y., Xu, A., Jin, X., Zheng, J., He, X., Cheng, Y., Xie, Q., Liu, R., 2018. Biosens. Bioelectron. 117, 422–428.
Sun, X., Lin, J., Guan, H., Li, L., Sun, L., Wang, Y., Miao, S., Su, Y., Wang, X., 2018. Appl. Catal., B 226, 575–584.
Sun, Y., Xu, B., Shen, Q., Hang, L., Men, D., Zhang, T., Li, H., Li, C., Li, Y., 2017. ACS Appl. Mater. Interfaces 9, 31897–31906.
Tang, C., Liu, Y., Xu, C., Zhu, J., Wei, X., Zhou, L., He, L., Yang, W., Mai, L., 2018. Adv. Funct. Mater. 28, 1704561.
Tian, H., Wang, S., Zhang, C., Veder, J.-P., Pan, J., Jaroniec, M., Wang, L., Liu, J., 2017. J. Mater. Chem. 5, 11615–11622.
Wang, Y., Jin, J., Chu, W., Cahen, D., He, T., 2018. ACS Appl. Mater. Interfaces 10, 15304–15313.
Wu, S., Tu, W., Zhao, Y., Wang, X., Song, J., Yang, X., 2018. Anal. Chem. 90, 14423–14432.
Xu, R., Lu, P., Wu, B., Wang, X., Pang, X., Du, B., Fan, D., Wei, Q., 2018. Sens. Actuators, B 274, 349–355.
Yan, P., Jiang, D., Tian, Y., Xu, L., Qian, J., Li, H., Xia, J., Li, H., 2018a. Biosens. Bioelectron. 111, 74–81.
Yan, X., Xu, Y., Tian, B., Lei, J., Zhang, J., Wang, L., 2018b. Appl. Catal., B 224, 305–309.
Zhang, Y., Xu, R., Kang, Q., Zhang, Y., Wei, Q., Wang, Y., Ju, H., 2018. ACS Appl. Mater. Interfaces 10, 31080–31087.
Zhao, G., Sun, M., Liu, X., Xuan, J., Kong, W., Zhang, R., Sun, Y., Jia, F., Yin, G., Liu, B., 2019. Electrochim. Acta 304, 334–341.
Zhou, Q., Xue, H., Zhang, Y., Lv, Y., Li, H., Liu, S., Shen, Y., Zhang, Y., 2018. ACS Sens. 3, 1385–1391.